System Characterization and Polarimetric Calibration of the Ku-Band Advanced Polarimetric Interferometer

Simone Baffelli[*1], Othmar Frey[1,2], Charles Werner[2], Irena Hajnsek[1,3]

[1]Earth Observation & Remote Sensing, ETH Zurich, Switzerland

[2]Gamma Remote Sensing, Gümligen, Switzerland

[3]Microwaves & Radar Institute, Oberpfaffenhofen, German Aerospace Center – DLR, Germany

[*]Email: baffelli@ifu.baug.ethz.ch

Abstract

This paper addresses the system characterization and the polarimetric calibration of the Ku-Band Advanced Polarimetric Interferometer (KAPRI). KAPRI is an FMCW ground-based real aperture radar system that uses slotted waveguide antennas. The rotation of the antennas introduces undesired phase ramps in azimuth. We present a geometrical model to account for this phase, and propose a method to correct it. Experimental data with a set of trihedral corner reflectors (TCR) in the scene was acquired with the system. A linear phase variation of 30 degrees was observed over the TCR which was geometrically modeled and successfully corrected.

1 Introduction

The Ku-Band Advanced Polarimetric Radar Interferometer (KAPRI) is an experimental ground-based FMCW real aperture radar (Figure 1). It operates at 17.2 GHz with a chirp bandwidth of 200 MHz, giving a range resolution of 0.75 m. Azimuth resolution is obtained using a slotted waveguide antenna with a beamwidth of $0.4°$.
KAPRI is a polarimetric extension of the Gamma Portable Radar Interferometer [1, 2].
In addition to the two standard modes of the GPRI, namely D-INSAR for measurement of line-of-sight displacements and single pass InSAR for digital elevation model generations, using KAPRI it is possible to acquire full polarimetric, interferometric datasets. This is of interest for several applications, especially for the observation of natural targets such as ice, snow or vegetation.
In this paper, we address a number of system-specific effects that have to be modeled and corrected to produce calibrated polarimetric data.

Figure 1: KAPRI during the first field test. The top two antennas are the H and V polarized transmitting antennas. The four bottom antennas correspond to the two receiving channels, each with a H and a V polarized antenna.

2 KAPRI: Data Acquisition and Imaging Procedure

Some of these effects are known from the previous experience with the regular GPRI, others are due to the modifications to the device and the antennas that permit polarimetric imaging. Thus, it is useful to first describe the general processing method that was previously used to obtain images with the GPRI.

2.1 Standard Processing Pipeline

In the range dimension, resolution is obtained with the FMCW principle[3] by transmitting a chirped signal while receiving. The received signal is then mixed with the signal being transmitted; a Fourier transform then allows to recover the range profile.
To separate scatters in the cross-range direction, a narrow beam emitted by a slotted array antenna is scanned in azimuth by mechanical rotation. During the rotation the data is oversampled in azimuth by using an angular step smaller than the antenna beamwidth, so that different realizations of the same signal can be decimated in azimuth by averaging adjacent samples before the range compression. This is done to increase the SNR of the measurement.
The processing of the data to obtain azimuth-resolved range profiles is made more complicated by the phased-array antennas: a deviation of the signal frequency from the design value will cause the antenna pattern to squint, reducing the effective azimuth resolution of the antenna [4]. To overcome this problem, at each frequency bin the dechirped samples are interpolated in azimuth to correct for the frequency-dependent azimuth beam squinting.
After this correction, the raw data is decimated in azimuth and then range-compressed using a Fourier transform [3].

2.2 Azimuthal Phase Ramp

With the standard GPRI, the range compressed data could be used directly to compute differential interferograms or elevation models.

Using KAPRI, when the phase of the undecimated range compressed data is analyzed, azimuthal phase ramps with different slopes for the HH and VV channels are observed (see Figure 5a and Figure 5c). This was not a problem when only one antenna type was employed, as this systematic effect was removed when computing phase differences between acquisitions in time or in space.

These ramps are potential source of errors for the polarimetric calibration and analysis: when data acquired with different antennas is combined coherently for polarimetry, the phase for the two channels do not cancel out and a residual variation in azimuth is observed.

The ramps are presumably caused by the fact that the phase center of the antennas are not positioned at the location of the rotation axis of the radar [5]. Additionally, the H and V antennas are not physically identical, such that potentially they have also different phase center locations along the slotted waveguide.

To model the effect of the shifted phase centers, the geometry of Figure 2 is used: an antenna is mounted at the end of a lever arm of length r_{arm}. The arm is rotated around the vertical axis at the other end to perform an azimuth scan of the beam. The antenna phase center has an horizontal displacement r_{ph} from the lever arm attachment.

We consider a point scatterer in the scene that has a range of closest approach r_{sl} when the phase center lies on the line connecting the point target to the lever arm rotation center.

Using this geometry, the phase of the signal scattered by the point target and measured at the antenna phase center during the scan as a function of the relative rotation from the closest approach, θ is:

$$\phi_{pt} = \frac{4\pi}{\lambda} R(\theta) \tag{1}$$

where $R(\theta)$ is the distance from the phase center to the point target.

To compute R, we apply the law of cosines on the green triangle in Figure 2: one side has length $c = r_{sl} + r_{ant}$ and the other r_{ant}. This length is the equivalent antenna rotation arm for a system with no phase center shift:

$$r_{ant} = \sqrt{r_{arm}^2 + r_{ph}^2}, \tag{2}$$

while the included angle θ is the rotation from the situation of closest approach:

$$R = \sqrt{c^2 + r_{ant}^2 - 2cr_{ant}\cos(\theta - \alpha)}. \tag{3}$$

The function is evaluated around the angle $\alpha = \arctan\frac{r_{ph}}{r_{arm}}$. This shift models the fact that for a displaced phase center the closest approach is not obtained when the target is in the center of the beamwidth, as shown in Figure 2. In this case, a faster phase variation is

expected because the cosine has a larger derivative in that region.

A scanning real aperture described by this model measures complex reflectivity range profiles $d(\theta_i, R)$ of a scene for the antenna rotation angles θ_i. For a point target at a fixed distance r_{sl} from the radar, due to Equation 3, the measured range R changes as a function of θ_i. Thus, the point scatterer response is observed to move through several range cells in the range compressed data. This variation in range is named **R**ange **C**ell **M**igration (**RCM**).

When the amount of range migration is much smaller than the range resolution, only the associated phase change (Equation 1) that produces the azimuthal phase ramp needs to be addressed. In the case of KAPRI, the former situation applies, otherwise more involved processing is required to realign the range samples to compensate for the RCM.
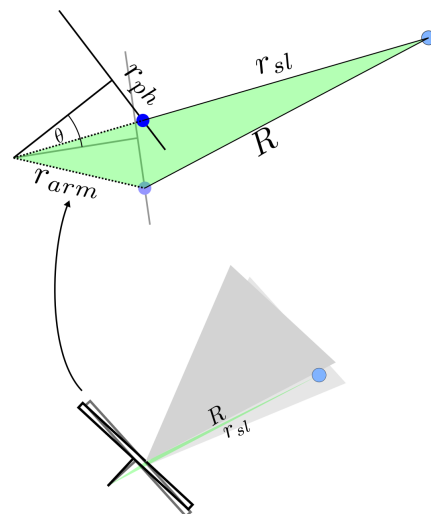
Figure 2: Geometry used for the derivation of the phase. r_{ph}: horizontal phase center displacement. r_{arm}: antenna lever arm. r_{sl}: range of closest approach. θ rotation angle from the situation at closest approach. R range to the point scatterer during the scan. The antenna beamwidth (gray triangle) is exaggerated.

In the geometrical model, the antenna phase center position in the coordinate system centered at the rotation axis is described by two parameters: the length of the antenna lever arm r_{arm} and the horizontal displacement of the phase center along the length of the antenna, r_{ph}. The first parameter is specified by the manufacturer or can be measured. This is not the case for r_{ph}; if the antenna has a large size and the wavelength is small, errors in the manufacturing of the antenna structure can result in significant displacements of the phase center from its intended location at the midpoint of the array. Therefore, we determine r_{ph} from the data by solving a nonlinear least squares problem:

$$\underset{(r_{ph}, \phi_{off})}{\arg\max} \|\phi_{meas} - \phi_{sim}\|^2. \tag{4}$$

Where $\phi_{sim} = \phi_{pt} + \phi_{off}$ is the simulated phase com-

puted using equation 1. A phase offset is added to model the unknown scattering and propagation phases of the target and the effect of noise. This is necessary in order to compute the correct value for r_{ph}, even though the estimated value for the phase offset will not be needed in the phase correction algorithm.

Once the parameter r_{ph} is determined, the model in Equation 3 can be used to derive a correction for the phase distortion. To do so, for each range line r_{sl} in the data, the measured azimuth samples $d(\theta, r_{sl})$ are convolved with a filter of the form:

$$f(\theta) = e^{J \frac{4\pi}{\lambda} (R(\theta, r_{sl}) - r_s l)} w(\theta).$$

(5)

Here w is a windowing function of length L_{int} that is necessary to limit the length of the integration; if this is not done, samples corresponding to different scatterers are combined coherently, degrading the azimuth resolution and the quality of the phase information.

By subtraction of $r_s l$ from R in Equation 5, the filter only corrects the phase ramp relative to the propagation phase at the range of closest approach. In this way that the correction does not alter the absolute phase of the signal.

The corrected, range compressed data is then:

$$d_{corr}(\theta, r_{sl}) = \int_{-\frac{L_{int}}{2}}^{\frac{L_{int}}{2}} e^{J \frac{4\pi}{\lambda} (R(\theta - \theta', r_{sl}) - r_{sl})} d(\theta') d\theta'.$$

(6)

This operation can be considered to be an modification of the azimuth decimation used for the standard GPRI processing, where $f(\theta)$ was a constant function.

2.3 Polarimetric Calibration

After the phase ramp correction, since the phase should only contain scattering and propagation contributions, the data can be calibrated for polarimetry.

Neglecting crosstalk between the channels, the measured scattering matrix for a pixel $\mathbf{S_{meas}}$ is assumed to be related to the theoretical matrix $\mathbf{S}$ by[6]:

$$\mathbf{S_{meas}} = \begin{bmatrix} S_{hh} & fge^{i(\phi_t)}S_{hv} \\ f/ge^{i(\phi_r)}S_{vh} & f^2 e^{i(\phi_r + \phi_t)}S_{vv} \end{bmatrix}$$

(7)

where f is the one-way copolar amplitude imbalance and g the crosspolar imbalance. $\phi_t = \phi_{t,v} - \phi_{t,h}$ is the phase imbalance when transmitting and $\phi_r = \phi_{r,v} - \phi_{r,h}$ is the receiver phase imbalance. The copolar amplitude imbalance f and $\phi_r + \phi_t$ are determined from the HH-VV intensity ratio and the phase difference measured at a corner reflector.

g and $\phi_t - \phi_r$ are estimated from the HV-VH amplitude ratio and phase difference averaged over all pixels in the scene. This estimation is based on the assumption of reciprocity for natural distributed targets.

Owing to the polarimetric acquisition mode used by KAPRI, the crosstalk can be neglected in first approximation: only one polarization is acquired at each pulse

by electronically connecting the desired transmitting and receiving antennas to the radar.

This method ensures a very high degree of polarization isolation between the channels. The isolation of the receiver has been measured by the manufacturer in the laboratory by connecting a delay line from the transmitter output to the input port for the H polarized antenna and leaving the V port disconnected. The minimum isolation observed for this configuration is in the order of 40 dB. Because only the co-polarized antenna pattern is known, it cannot be excluded that a certain amount of crosstalk is caused by the antennas having cross-pol sidelobes in the direction of copolar main lobe.

Because the calibrated data appears to have a good polarimetric quality, the determination and correction of the crosstalk may not be strictly necessary.

3 Experimental Data and Results

For the characterization and calibration of KAPRI, a full polarimetric dataset of a scene containing five **T**rihedral **C**orner **R**reflectors (**TCR**) was acquired; their location is marked in Figure 4.

The system is equipped with a 2 meters long slotted waveguide antenna with a beamwidth of $0.4°$. The antenna is mounted on a lever arm of length $r_{arm} = 0.25$ m with respect to the vertical rotation axis of the system. During the test, the antenna was rotated in increment of $0.01°$.
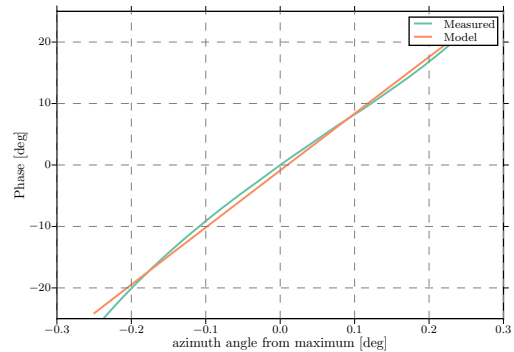
Figure 3: Unwrapped azimuthal phase for the TCR, VV channel. The blue line is the measured phase, the green line the phase computed using the model, with an estimated horizontal phase center offset $r_{ph} = 12cm$.
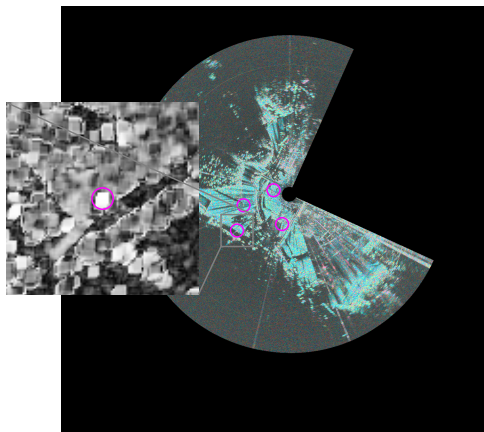
Figure 4: Geocoded intensity and phase of the HH-VV covariance matrix element after correction and polarimetric calibration. The reflectors location is marked with magenta circles. The inset figure shows the HH-VV coherence in the vicinity of a TCR.

(a) Before phase correction (HH channel).

(b) After phase correction (HH channel).

(c) Before phase correction (VV channel).

(d) After phase correction (VV channel).

Figure 5: Oversampled phase response of a trihedral corner reflector. Range is horizontal, azimuth is vertical. One color cycle corresponds to a phase change of 2π. The intensity is coded in the brightness. The phase at the peak was subtracted from each response for a better comparison of the phase ramps.

3.1 Azimuth Phase Ramp

The polarimetric response of the range compressed data was then analyzed; the first step being the computation of the HH-VV phase difference. When examining it, an unexpected phase ramp in azimuth direction was observed at the reflectors. The ramp was mainly caused by a very pronounced linear phase trend in the VV channel (Figure 5c). To explain this behavior the geometrical model of subsection 2.2 was developed and tested on the TCRs: the range and azimuth coordinates corresponding to the reflectors were identified and the samples included in the antenna 3dB beamwidth where extracted and used to compute r_{ph} with the method described in subsection 2.2. The resulting horizontal phase center displacement r_{ph} is 12 cm for the VV channel and 2 cm for the HH channel. The measured and modeled unwrapped phase for one reflector in the VV channel is plotted in Figure 3 alongside with the simulated phase, a good fit can be observed.

Using the estimated value for r_{ph} the data was corrected according to Equation 5, with an integration length L_{int} corresponding to $0.7°$. It was observed that a that a longer integration window leads to a better phase response at the cost of a reduced azimuth resolution. In Figure 5 the oversampled phase and amplitude responses of a TCR for the HH and VV channel are displayed before and after the correction.

To allow a more precise analysis, the phase response for all TCRs at the range of maximum intensity is plotted for the VV channel in Figure 6. The plot for the HH is not shown as the variation was much smaller in that case. For an easier comparison of the phase variation, the phase at the maximum amplitude was subtracted from each curve. The uncorrected data shows an azimuth phase ramp with a variation of approx. $30°$ inside the antenna beamwidth. The reflectors at 107 and 299 meters have a non-linear response that cannot be explained by the model. The nearer target was presumably not in the full far field region of the radar, which starts approx. 500 m. The corner reflector at 299 m was intentionally obscured by placing it behind a row of trees; its response may contain a contribution by the two way propagation of the beam through the obscuring trees and back to the radar.

In all cases, the phase ramp has been reduced to under $10°$ by the correction. The two reflectors at 107 and 499 showing the biggest residual variation, this result is to be expected because they show an uncorrected phase ramp that is not well explained by the model. Finally, we observe that because of the integration in azimuth, the amplitude response is broadened resulting in a angular resolution of approx $0.7°$.
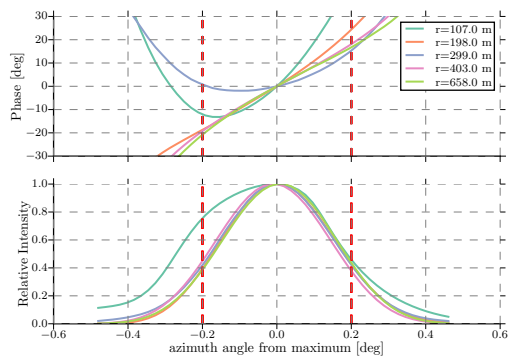
(a) Before phase correction.
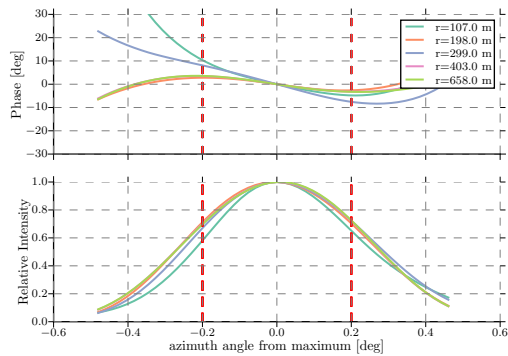
(b) After phase correction.

Figure 6: Phase and amplitude response for the TCRs in the VV channel. The phase at the maximum has been subtracted to make the two curves comparable. The red lines indicate the width of the antenna beamwidth. The phase variation is under $10°$ after the proposed correction, the residual change being mostly outside of the antenna beamwidth.

3.2 Polarimetric Analysis

After the correction of the azimuthal phase ramp, the polarimetric calibration parameters were determined using the procedure described in subsection 2.3. The validity of the polarimetric calibration is verified by computing polarization signatures[7] for the trihedral reflectors. In Figure 7 the co-polarised amplitude response for two TCRs before and after the calibration are shown. The uncalibrated signature is so distorted that it cannot be connected with any ideal scattering mechanism. After the phase and imbalance compensation, the response is much closer to the expected signature for perfect odd bounce scattering, supporting the validity of the proposed correction and calibration method.
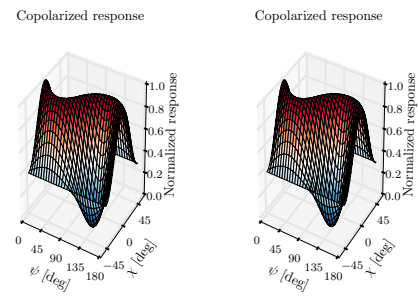
(a) Uncalibrated
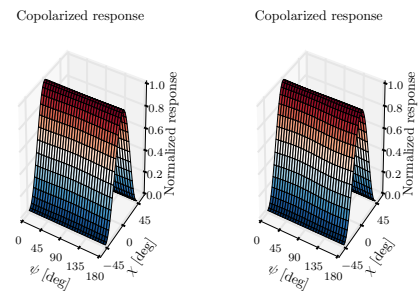
(b) Calibrated

Figure 7: Co-polarized signature for two trihedral corner reflectors. Figure 7a before the polarimetric calibration, Figure 7b after the polarimetric calibration procedure.

4 Conclusions

In this paper, we addressed aspects of the system characterization required for the full polarimetric calibration of KAPRI, the new ground-based Ku-band interferometric FMCW radar. In particular, we discussed a geometrical model to explain azimuthal phase variation of point target responses in the range-compressed data. An antenna phase center which is displaced with respect to the lever arm is assumed. This induces a slight variation in range during the scan and thus a phase modulation in the phase of point scatterers. This phase complicates the polarimetric calibration of the device by introducing a phase term unrelated to scattering or propagation in the acquired data.

Using a geometrical model, we can estimate the location of the phase center in the antenna and correct the phase ramp by coherently combining azimuth samples with an appropriate, range-dependent phase correction factor. This produces data where the azimuth phase response of point targets is stable within the 3 dB beamwidth of the antenna.

After this correction, a polarimetric calibration technique[6] was applied to correct phase and amplitude imbalances, producing calibrated full polarimetric data. The calibration was verified using the polarization responses of trihedral corner reflectors. The signatures of the corrected data were similar to the expected response for ideal trihedral reflectors.

References

[1] C. Werner, A. Wiesmann, T. Strozzi, A. Kos, R. Caduff, U. Wegmuller, and U. Wegmüller, "The GPRI multi-mode differential interferometric radar for ground-based observations," in *EUSAR 2012*. VDE, 2012, pp. 304–307. [Online]. Available: http://ieeexplore.ieee.org/stamp/stamp.jsp?arnumber=06217065

[2] C. Werner, T. Strozzi, A. Wiesmann, and U. Wegmulle, "A real-aperture radar for ground-based differential interferometry," *International Geoscience and Remote Sensing Symposium (IGARSS)*, vol. 3, no. 1, pp. 210–213, jul 2008.

[3] A. Stove, "Linear FMCW radar techniques," *IEE Proceedings F Radar and Signal Processing*, vol. 139, no. 5, p. 343, oct 1992. [Online]. Available: http://digital-library.theiet.org/content/journals/10.1049/ip-f-2.1992.0048

[4] B. Sarkar, R. Roy, and C. Reddy, "Deterioration in resolution of a radar using long slotted waveguide antenna," in *Digest on Antennas and Propagation Society International Symposium*, jun 1989, pp. 1740–1742. [Online]. Available: http://ieeexplore.ieee.org/lpdocs/epic03/wrapper.htm?arnumber=135070

[5] H. Lee, J.-H. Lee, K.-E. Kim, N.-H. Sung, and S.-J. Cho, "Development of a Truck-Mounted Arc-Scanning Synthetic Aperture Radar," *IEEE Transactions on Geoscience and Remote Sensing*, vol. 52, no. 5, pp. 2773–2779, may 2014. [Online]. Available: http://ieeexplore.ieee.org/lpdocs/epic03/wrapper.htm?arnumber=6553134

[6] A. G. Fore, B. D. Chapman, B. P. Hawkins, S. Hensley, C. E. Jones, T. R. Michel, and R. J. Muellerschoen, "UAVSAR Polarimetric Calibration," *IEEE Transactions on Geoscience and Remote Sensing*, vol. 53, no. 6, pp. 3481–3491, jun 2015.

[7] J. J. van Zyl, H. A. Zebker, and C. Elachi, "Imaging radar polarization signatures: Theory and observation," *Radio Science*, vol. 22, no. 4, pp. 529–543, 1987. [Online]. Available: http://dx.doi.org/10.1029/RS022i004p00529